

## ELECTROCHEMICAL AND STRUCTURAL STUDY OF ZINC-RICH BRASS DEPOSITED FROM PYROPHOSPHATE ELECTROLYTE ONTO THE CARBON STEEL

M. Y. HACİİBRAHİMOĞLU<sup>a,\*</sup>, A. YAVUZ<sup>a</sup>, M. ÖZTAŞ<sup>b</sup>, M. BEDİR<sup>c</sup>

<sup>a</sup>*Department of Metallurgical and Materials Engineering, Gaziantep University,  
Sehitkamil, 27310, Gaziantep, Turkey*

<sup>b</sup>*Department of Chemistry and Process Engineering, Yalova University, 77100,  
Yalova, Turkey*

<sup>c</sup>*Department of Physics Engineering, Gaziantep University, Sehitkamil, 27310,  
Gaziantep, Turkey*

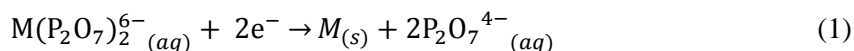
Alkaline pyrophosphate electrolyte was used for the deposition of brass including different proportions of Zn and Cu onto carbon steel substrate to determine the mechanism of the growth and striping of Cu, Zn and their alloys. Zinc-rich brasses were obtained potentiostatically and the behaviour of resulting films was studied potentiodynamically in terms of redox processes and corrosion studies they have. Deposition and dissolution mechanisms of Zn are independent of the film thickness. However, these mechanisms of brasses depend not only on the film thickness but also the Zn content. The corrosion resistivity of brass can be optimised and it can reach up to 27 times more effective than pure Zn due to the content of metals in alloy and the alloy structure. Micro-lamellar structure of brasses was also observed in the alloy containing  $57.5 \pm 0.50\text{wt\%}$  Zn.

(Received January 15, 2016; Accepted March 9, 2016)

**Keywords:** Copper-zinc alloy, Electrodeposition, Pyrophosphate electrolyte,  
Micro-lamellar structure, Corrosion

### 1. Introduction

Besides decorative purposes [1,2], brass coatings are required to protect the substrates against aggressive environments such as lubricant, gaseous and liquid environments resulting in performance and lifetime reduction [3,4]. Until recently, cyanide based electrolyte has been used for brass deposition [5-7]. However, this is no longer desirable because of environmental and safety issues. Therefore, several research groups have attended to study cyanide free and environmentally friendly medium such as ionic liquids [8,9] or aqueous medium (tartrate [10], gluconate [11], EDTA [12], ammonia [13], pyrophosphate [14,15], based ligand solution). The complexing agents in the deposition baths do not significantly affect the deposition potentials of zinc but copper. Among non-cyanide aqueous electrolyte, pyrophosphate bath is an attractive ligand to obtain brass coating. Kravtsov et al. [16] and Konno et al. [17] showed that the deposition mechanism of pure metals ( $\text{Cu}^{2+}$ ,  $\text{Zn}^{2+}$   $\text{Pb}^{2+}$  and  $\text{Sn}^{2+}$ ) with pyrophosphate complexing agent is:



Brass film was obtained with the same mechanism in several works [16,18-20], however Vagramyan et al. [6] claimed that the brass deposition with this ligand had some problems

---

\*Corresponding author:yakup@gantep.edu.tr

including cracked and low zinc-content film. Fujiwara et al. and Juškėnas et al. [21,22] later on illustrated that lower deposition potential could result in the zinc-rich brasses. Although there are many studies regarding electrochemical deposition and characterization (structural, optical and anti-corrosion behaviors) of copper-rich brass ( $\alpha$ -brass) [23-27], preparation and characterization of zinc-rich brass ( $\beta$  and  $\gamma$ -phases of brass) have not been studied widely.

Improving the surface of alloy means achieving better wear, abrasion and corrosion resistance. Corrosion resistivity of steels is an important factor in engineering applications. One of the objective of this work is to examine the anti-corrosive effect of brass onto carbon steel with variable high zinc content.

The main objective here is to understand the electrochemical mechanism of brass deposition onto the carbon steel upon changing content of brass. Potentiodynamic data of pure Zn and pure Cu are collected to determine the similarities and contrast of pure Zn and pure Cu coatings with brass films. Another objective is to explore the structure of the film deposited with different ratio of Zn and Cu in pyrophosphate electrolytes. It is also aimed to determine and optimize the variation of anti-corrosion behaviour of brass as a function of Zn/Cu ratio in solid form.

## 2. Experimental

The solutions for all experiments were prepared from chemicals supplied by Sigma-Aldrich with distilled water ( $<10 \mu\text{S cm}^{-1}$ ). 0.2 M CuSO<sub>4</sub> and 0.2 M ZnSO<sub>4</sub> compounds were individually added into the solution containing 0.9 M K<sub>4</sub>P<sub>2</sub>O<sub>7</sub> and 0.07 M KH<sub>2</sub>PO<sub>4</sub> (referred as background electrolyte) for pure Cu and pure Zn deposition, respectively. The concentration of Zn<sup>2+</sup> in the background electrolyte is constant (200 mM) for brass deposition. However, Cu<sup>2+</sup> concentration in the electrolyte was varied according to the following values: 50 mM, 100 mM, 150 mM and 200 mM as shown in Table 1. The value of pH for these solutions was measured as  $8.5 \pm 0.3$ . The solutions containing both metal compounds are listed in Table 1 with their labels.

*Table 1: Chemical contents of electrolytes with their labels.*

Solution Code	CuSO <sub>4</sub> (mM)	ZnSO <sub>4</sub> (mM)	K <sub>4</sub> P <sub>2</sub> O <sub>7</sub> (M)	KH <sub>2</sub> PO <sub>4</sub> (M)
Cu50-Zn200	50.0	200	0.90	0.07
Cu100-Zn200	100	200	0.90	0.07
Cu150-Zn200	150	200	0.90	0.07
Cu200-Zn200	200	200	0.90	0.07

A three-electrode cell was used in potentiodynamic experiments either cyclic voltammetry for studying electrochemical mechanism or linear sweep voltammetry for corrosion study. AISI 4140 steel (carbon steel) which has disc shaped made out of 1 cm diameter with one side covered bakelite was used as the working electrode. The auxiliary electrode was Pt flag (2 cm<sup>2</sup>). All the potentials in the work presented in this paper were referred to Ag/AgCl (sat. KCl) reference electrode. Before the deposition of brass, the surface of carbon steel was mechanically polished to obtain a mirror shine surface using sandpaper having grid size varied from 400 to 3000 then sonicated solution for 5 minutes and finally rinsed with deionised water.

The electrochemical experiments were carried out in a CHI 1100 potentiostat (CHI Instruments Inc., USA). The coatings were obtained potentiostatically at -2.0 V for 300 seconds. The resulting films were transferred to 3wt% NaCl to measure corrosion resistivities. All experiments were conducted at room temperature ( $20 \pm 2$ ). The elemental analysis of the brass was carried out by scanning electron microscope JEOL 6400 with energy dispersive spectrometer performing between 15 and 30 kV.

### 3. Results

#### 3.1 Electrodeposition Mechanism of Brass

##### 3.1.1 Deposition of Pure Cu and Pure Zn Metals

Before starting the analysis of brass deposition, the electrochemical growth of Cu and Zn is studied by the cyclic voltammetry and presented in Figure 1.

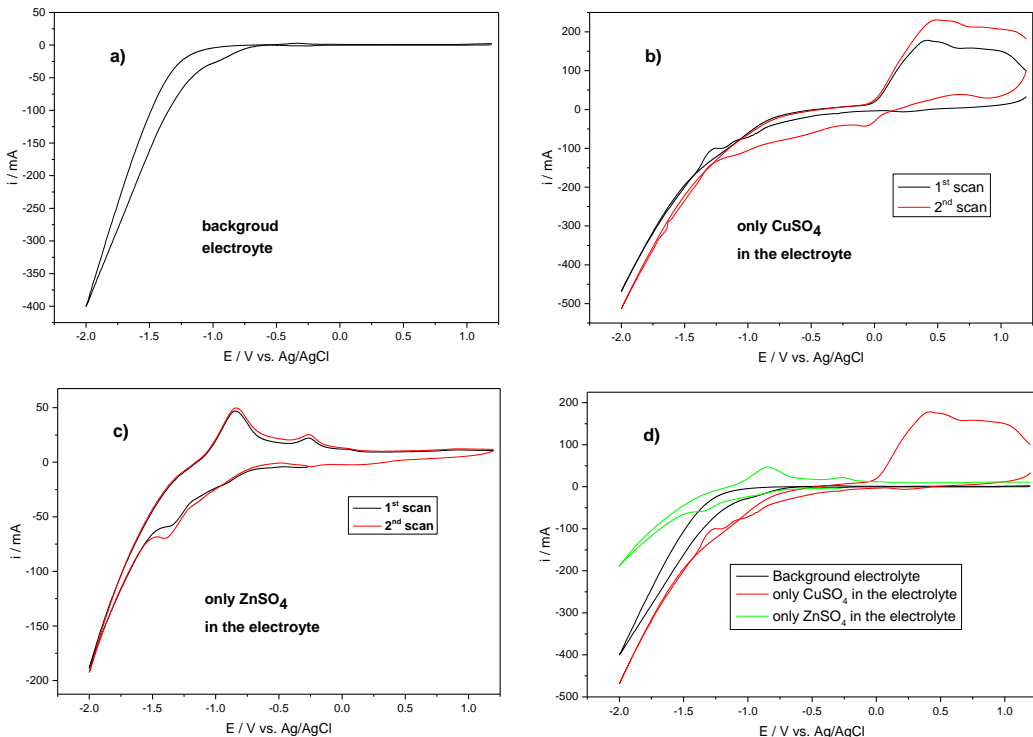


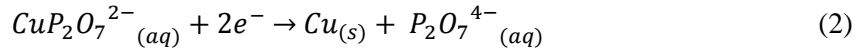
*Fig. 1: Cyclic voltammogram of a) background electrolyte ( $0.90 \text{ M } K_4P_2O_7 + 0.07 \text{ M } KH_2PO_4$ ); b) pure Cu containing system ( $0.20 \text{ M } CuSO_4$  in the electrolyte); b) pure Zn containing system ( $0.20 \text{ M } ZnSO_4$  in the electrolyte); d) all data given in panel a, b and c. CV data recorded for the steel working electrode at a sweep rate of  $50 \text{ mV s}^{-1}$ .*

The copper, zinc and brass reduction and deposition processes have been previously studied in non-cyanide medium onto the Pt [6] and Au [15] working electrode, however the deposition process onto the steel has not been studied widely. As there is no reaction of iron (steel) in pyrophosphate medium at the potential window from 1.2 to  $-1.0 \text{ V}$  given in Figure 1a, the steel substrate can be safely used as working electrode. The reduction of hydrogen is seen around  $-1.0 \text{ V}$  in Figure 1a. The starting potential was selected where there is no current flow at  $1.2 \text{ V}$ . As the brass films were obtained potentiostatically by applying  $-2 \text{ V}$ , the potential range was selected up to  $-2 \text{ V}$  on the cathodic direction in order to observe the probable dynamics and mechanisms of electrochemical process of brass deposition. Additionally, the steel was used as a working electrode for cyclic voltammograms study because the ions could behave varied on different substrate depending mainly on the crystal structure [22]. Therefore, steel substrate was used as the working electrode to obtain better characterisation of the brass deposition.

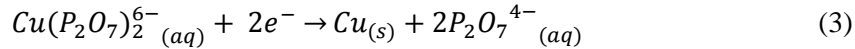
Figure 1b does not show any reduction peak until  $-1.0 \text{ V}$  which indicates that there is no Cu reduction until that potential. Although the reduction of  $Cu^{2+}$  ions begins normally at a very earlier potential, here pyrophosphate ions cause the reduction potential of  $Cu^{2+}$  to shift to more negative direction at  $-1.1 \text{ V}$ .

It is known that during deposition of metals some free  $OH^-$  ions are appeared in aqueous cyanide medium because of hydrogen evolution and thus some metalhydroxide can be deposited

as well [6] but the general mechanism for copper deposition in pyrophosphate medium proposed by Konno et al. [17] is as follow:



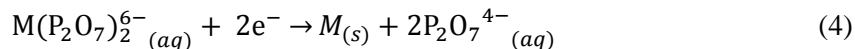
Konno et al. also proved that the mechanism can be different depending on the concentration of pyrophosphate in the electrolyte for example at high concentration of pyrophosphate (>0.18 M), the mechanism becomes:



There is a peak at -1.2 V which is attributed to copper deposition (see Figure 1b). The linearly decreasing of reduction current given in Figure 1a and Figure 1b shows similarities, therefore around this potential, hydrogen evolution reducing the current efficiency also occurs with copper deposition. The cyclic voltammogram of copper reduction ( $\text{CuSO}_4$  in the background electrolyte) and hydrogen reduction (just background electrolyte) are compared in Figure 1d. As expected, the charge (area under the peak) of copper solution is higher than that of the background electrolyte itself because Cu deposition is associated with hydrogen evolution [16]. On the reverse direction, copper differently shows two oxidation peaks as the ligand does not affect oxidation of solid Cu. One of them starts at -0.1 V, which is related to the dissolution of Cu film. This is probably  $\text{Cu}^0/\text{Cu}^+$  oxidation because the other oxidation peak which is around 0.8 V can be connected  $\text{Cu}^+/\text{Cu}^{2+}$  oxidation. The broadness of the oxidation peak could exist due to the interference of both oxidation reactions  $\text{Cu}^0/\text{Cu}^+$  and  $\text{Cu}^+/\text{Cu}^{2+}$ . While there is no reduction peak in the first scan until -1.2 V, there is a small reduction peak around 0 V in second scan shown in Figure 1b. This can be attributed to the reduction of  $\text{Cu}^{2+}/\text{Cu}^+$  (indeed  $\text{Cu}(\text{P}_2\text{O}_7)_2^{6-}/\text{Cu}(\text{P}_2\text{O}_7)_2^{7-}$ ) as the surface of steel working electrode now has been changed with the deposition of some copper.

Figure 1c shows the cyclic voltammogram curve of  $\text{ZnSO}_4$  in pyrophosphate medium. There is no reduction until -1.1 V which is exactly the same as just that of background electrolyte. The cyclic voltammogram of Zn deposition differs from hydrogen evolution as the potential of -1.3 V, at which the zinc nucleation takes place, is proceeded (given in Figure 1d). After a small plateau around -1.4 V, hydrogen evolution and Zn deposition are differentiated. The striking feature of these curves is that the charge of zinc deposition is lower than that of the background electrolyte. While zinc deposition and hydrogen evolution occurs concurrently, the expectation was that the charge for zinc deposition would be higher than that for just hydrogen evolution (background cycling) as it has been observed in copper deposition. However, the steel working electrode with zinc deposition reduces hydrogen evolution on the substrate because new surface, probably, is covered partly with zinc. Therefore, zinc coating blocks the active surface area and the amount hydrogen evolution is lessened.

Zinc deposition also can be accepted to have the same mechanism similar to the deposition of Cu in the same electrolyte which is accepted for other metals ( $\text{Pb}^{2+}$  and  $\text{Sn}^{2+}$ ) shown by Kravtsov et al [16]. As the concentration of pyrophosphate is higher in this case (0.9 M), the mechanism must be:



Here, M (Metal) represents Zn. Striping of Zn has different mechanism as it has two significant oxidation peaks. The first one (around -0.9 V) must be attributed to  $\text{Zn}^0/\text{Zn}^+$  oxidation and the other one (around -0.3) must be due to  $\text{Zn}^+/\text{Zn}^{2+}$ .

### 3.1.2 Deposition of Brass

The complexing agents in the electrolyte do not significantly affect the deposition potentials of zinc but copper is affected largely by the agents. Therefore, ligand of  $\text{P}_2\text{O}_7^{4-}$  was chosen to deposit Cu with Zn [7]. There are plenty of work related to brass films which are mainly focus on applications and characterisations of brass [12,28-31]. However, the cyclic voltammetric

analysis of brass on steel substrate is required to go into details. Figure 2 illustrates how content of copper ions in the electrolyte affects the cyclic voltammogram responses when the brass deposits onto the steel working electrode.

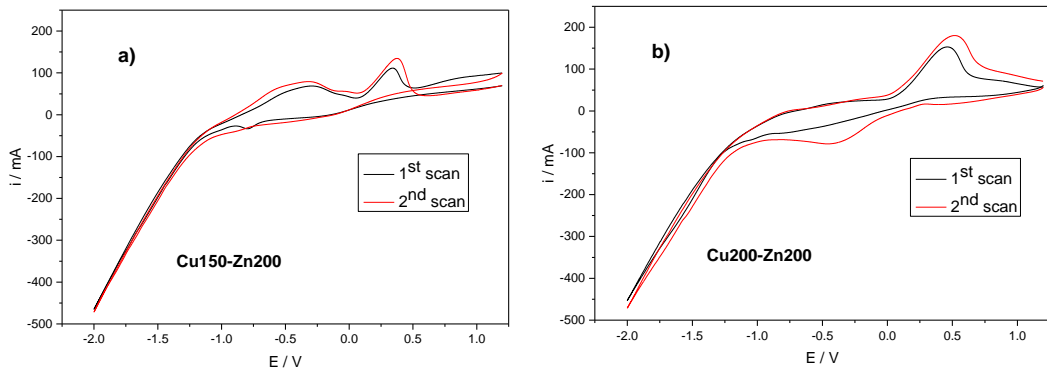
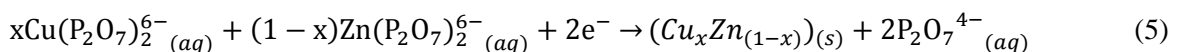


Fig. 2: Cyclic voltammogram of deposition solution data for a) the Cu150-Zn200 solution; b) the Cu200-Zn200 solution. ( $v = 50 \text{ mVs}^{-1}$ )

The cyclic voltammogram curves for all brass solutions in this study indicate that all brass films start to deposit around -1.2 V the same as Cu deposition (see Figure 1b) and until -1.2 V there are not any reduction peak as given in Figure 2.

The reduction of  $\text{Cu}^{2+}$  or  $\text{Zn}^{2+}$  (in the form of  $\text{Cu}(\text{P}_2\text{O}_7)_2^{6-}$  and  $\text{Zn}(\text{P}_2\text{O}_7)_2^{6-}$ , respectively) simultaneously occurs with hydrogen evolution which causes a significant decrease in current efficiency [15]. There are both hydrogen evolution and copper deposition simultaneously at potential interval more negative than -1.2 V and hydrogen evolution with zinc deposition at around -1.4 V. In literature it is known that when more negative external potential is applied through the electrolyte containing copper and zinc salt, the brass films include higher ratio of zinc [21,22], therefore -2 V was selected in order to obtain Zinc-rich brass for corrosion study.

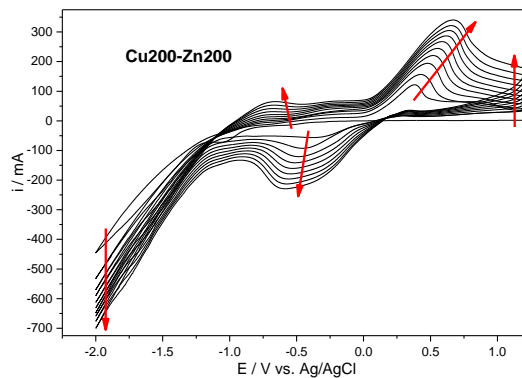
The mechanism of brass deposition must be the combination of Cu and Zn deposition. Therefore the mechanism can be shown as follows:



$x$  is the mol fraction of copper in the brass depending on deposition time, electrolyte, potential and current applied to the system [14,32-34].

All of the cyclic voltammogram studies of brass in this work show one oxidation peak at first scan (Cu200-Zn200 is given as a representative example). However, among all these cyclic voltammogram (Cu50-Zn200, Cu100-Zn200, Cu150-Zn200 and Cu200-Zn200), only Cu150-Zn200 has two oxidation peaks given in Figure 2a. The first oxidation peak at -0.4 for Cu150-Zn200 solution can be attributed to  $\text{Zn/Zn}^+$  ( $\text{Zn}$  to  $\text{Zn}(\text{P}_2\text{O}_7)_2^{7-}$ ) transformation. The change of  $\text{Zn}$  to  $\text{Zn}^+$  was around -0.9 V in pure zinc electrolyte. This difference is because of new type of film as there is copper content in the brass. The second oxidation peak around 0.3 V for the Cu150-Zn200 must be related to remaining brass striping to  $\text{Zn}^{2+}$  and  $\text{Cu}^{2+}$  ( $\text{Zn}(\text{P}_2\text{O}_7)_2^{6-}$  and  $\text{Cu}(\text{P}_2\text{O}_7)_2^{6-}$ ). However, the cyclic voltammograms for other solutions (Cu50-Zn200, Cu100-Zn200 and Cu200-Zn200) do not have  $\text{Zn/Zn}^+$  oxidation and directly all Cu and Zn become  $\text{Cu}^{2+}$  and  $\text{Zn}^{2+}$  as shown in Figure 2b. The differences between Cu150-Zn200 and others can be related to the amount of Zn content in the brass. This can be addressed by EDAX analysis given in section 3.2.1.

While the reduction of Cu200-Zn200 electrolyte on steel electrode is not seen until -1.2 in the first scan, a reduction peak around -0.4 rises on the second scan due to the change on steel electrode which now could have little brass on top of it. This requires a detail analysis, hence Figure 3 shows the consecutive cycling of Cu200-Zn200 electrolyte on the steel working electrode.



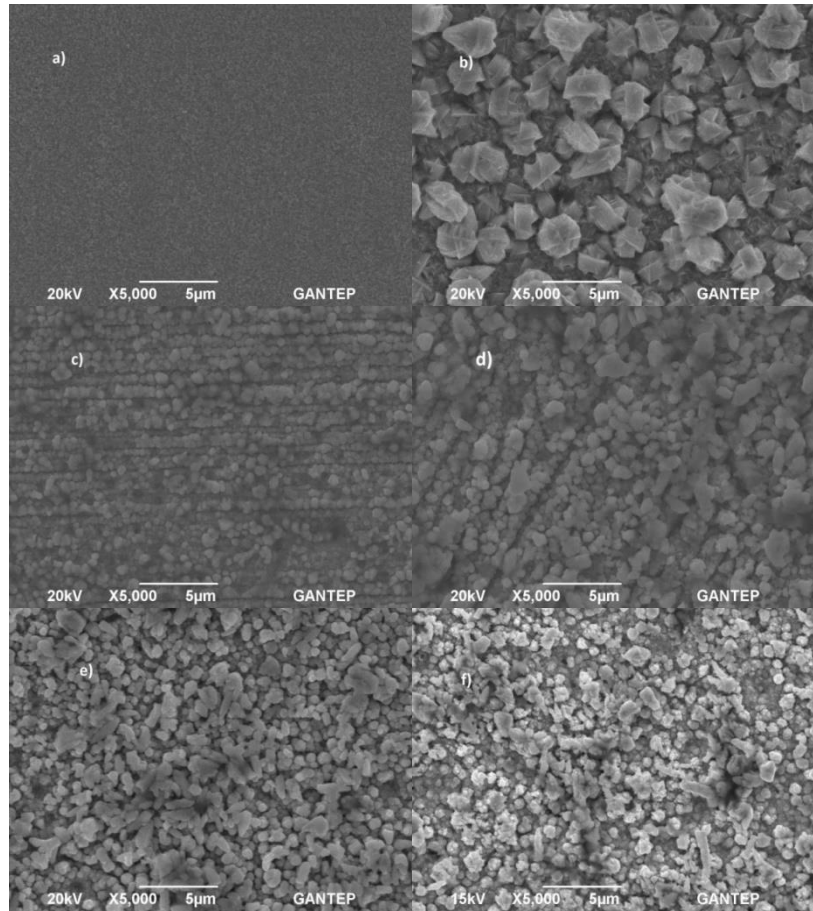
*Fig. 3: Consecutive cycling on the steel working electrode for the Cu200-Zn200 solution ( $v = 50 \text{ mVs}^{-1}$ ). The arrows indicate the change of current upon increasing the number of scans.*

Figure 3 shows that the current of each cycle increases at 1.2 V indicating deposited brass cannot be stripped 100% and the surface population of brass film increases after each cycle. As film is getting thicker which can be understood from the rising of the oxidation and reduction peaks upon increasing the number of scans, one more reduction and oxidation peak appear around -0.5 V and -0.7 V, respectively given in Figure 3. The first reduction peak appearing with increasing the numbers of scans is attributed to  $\text{Cu}^{2+}/\text{Cu}^+$  (in the form of  $\text{Cu}(\text{P}_2\text{O}_7)_2^{6-}/\text{Cu}(\text{P}_2\text{O}_7)_2^{7-}$ ) reduction as seen in the second cycle of Figure 1b and Figure 2b. The other peak (oxidation peak) is seen because of the oxidation of  $\text{Zn}/\text{Zn}^+$  ( $\text{Zn}$  solid to  $\text{Zn}(\text{P}_2\text{O}_7)_2^{7-}$ ) similar to the cyclic voltammogram obtained from the electrolyte containing only zinc solution (without copper solution) given in Figure 1c. This consecutive cycling confirms how the mechanism of deposition and striping of brass are differentiated depending on brass thickness, consequently composition and structure of the electrode. While the early stage of brass deposition consists of just the reduction of  $\text{Cu}^{2+}$  (indeed  $\text{Cu}(\text{P}_2\text{O}_7)_2^{6-}$ ) and  $\text{Zn}^{2+}$  ( $\text{Zn}(\text{P}_2\text{O}_7)_2^{6-}$ ) to  $\text{Cu}_x\text{Zn}_{(1-x)}$  alloy directly onto the steel electrode, later on -at subsequent scans-  $\text{Cu}^{2+}$  ( $\text{Cu}(\text{P}_2\text{O}_7)_2^{6-}$ ) reduces  $\text{Cu}^+$  ( $\text{Cu}(\text{P}_2\text{O}_7)_2^{7-}$ ) just before solid Cu deposition onto the new electrode which has some nucleation and growth of thin brass film. On the other hand the stripping mechanism of thin brass film (at the early stage of cycling) contains directly the oxidation of Zn-Cu to  $\text{Zn}^{2+}-\text{Cu}^{2+}$  (as  $\text{Cu}(\text{P}_2\text{O}_7)_2^{6-}$  and  $\text{Zn}(\text{P}_2\text{O}_7)_2^{6-}$ ), however solid zinc in thicker brass (subsequent cycles) firstly is oxidised to  $\text{Zn}^+$  ( $\text{Zn}(\text{P}_2\text{O}_7)_2^{7-}$ ) ions and the remaining film later on strips with increasing potential. This can provide new possibilities to control the composition of brass by potential change.

### 3.2 Characterization of Brass Films

#### 3.2.1 Morphology of Brass Films

Figure 4 shows SEM micrographs of pure Cu, pure Zn and their alloy consisting of different proportions of both metals. Cu and Zn proportions in brass film obtained from EDAX analysis are listed in Table 2.



*Fig. 4: SEM images of a) pure Cu coating; b) pure Zn coating; and brass coating obtained from c) the Cu50-Zn200; d) the Cu100-Zn200; e) the Cu150-Zn200; f) the Cu200-Zn200 solitions.*

While pure Cu film on carbon steel is smooth and its grain size is much less than 1 μm, the average grain size of the deposited pure Zn is 2.3 μm. Defects or crackings of the coating layer were not observed for any film presented here. The structure of brass is changed with variable Cu ratio in the electrolyte caused to the different ratio of metals in brass shown in Figure 4. It is indicated that the size of  $\text{Cu}_x\text{Zn}_{(1-x)}$  crystallites has generally regular spherical morphology with a size range of ca. 0.5-2 μm, however the pattern of them are so different.

Although the patterns of the solid obtained from the Cu50-Zn200 and the Cu100-Zn200 have a highly oriented lamellar structure, those of Cu150-Zn200 and Cu200-Zn200 have nodular structure of micrograins (at random orientation). To our knowledge, these micro-lamellar structures of any alloys have not been obtained previously from any method conducted at room temperature. It is known that normally this kind of micro-lamellar structure of alloys occurs at a eutectic point where alloy phases start to solidify at a high temperature [35,36]. Nano-lamellar structures were observed in several studies for example: Zr-Nb [37], Cu-Al [38], Co-W [39] and Ti-Al [40].

Table 2 displays that the ratios of Cu and Zn elements in brass do not have the same trend with the ratios of  $\text{CuSO}_4$  and  $\text{ZnSO}_4$  solutions in the electrolyte using for brass deposition. For instance, Cu ratio in brass obtained from the Cu150-Zn200 is lower than that of the Cu100-Zn200 while the concentration of  $\text{CuSO}_4$  is higher in the Cu150-Zn200 electrolyte (150mM  $\text{CuSO}_4$  + 200 mM  $\text{ZnSO}_4$ ) than the Cu100-Zn200 electrolyte (100mM  $\text{CuSO}_4$  + 200 mM  $\text{CuSO}_4$ ). On the other hand, the ratios of Zn in solid form of brasses obtained from the Cu50-Zn200 and the Cu100-Zn200 electrolyte have almost the same, 57% and 58% respectively. Figure 4c and Figure 4d illustrating the same microstructure of the brasses obtain from the Cu50-Zn200 and the Cu100-Zn200 can have a relationship with the content ratio given in Table 2.

Table 2: Contents of Zn and Cu elements in brass obtained from EDAX analysis of the films.

Sample	Zn (wt% in brass)	Cu (wt% in brass)
Cu50-Zn200	57	43
Cu100-Zn200	58	42
Cu150-Zn200	66	34
Cu200-Zn200	50	50

Figure 5 shows the phase diagram of the Cu-Zn system. There are seven solid phases depending on the ratio of the elements and the temperature illustrated in Figure 5. Among them,  $\beta'$ -phase is seen around 50% zinc content. As the zinc content is increased,  $\gamma$ -phase is formed. As the Zn content in the Cu50-Zn200 and the Cu100-Zn200 is  $57.50 \pm 0.50\%$  which have also lamellar structure (see Table 2 and Figure 4c - Figure 4d),  $\beta'$ -phase and  $\gamma$ -phase could be solidified around this percentage of Zn in brass. Therefore, red line in Figure 5 shows the probable border of  $\beta$ -phase and  $\gamma$ -phase transition or  $\beta+\gamma$ -phase and  $\gamma$ -phase transition. Weston et al [39] observed nanolamellar structure in Co-W coating and explained it with the spinodal decomposition during the deposition process.

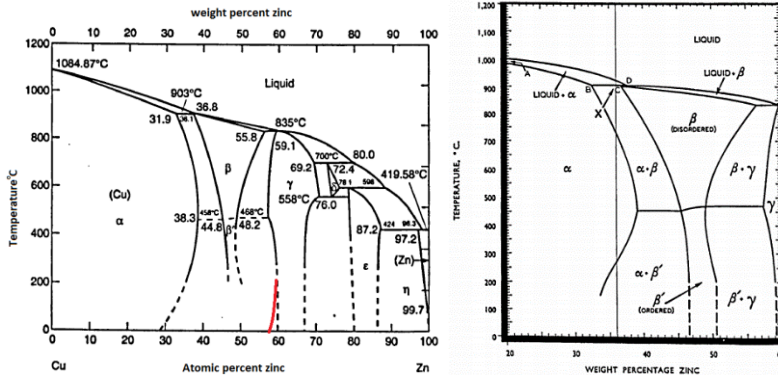


Fig. 5: a) phase diagram for Cu-Zn; b) higher magnification between 20-60% of Zn [41].

All the studies regarding lamellar structure of allow in the literature were obtained with heat treatment. Cadirli et al. solidified Pb-Sn eutectic samples in a furnace under an argon atmosphere [42]. Ti-6Al-3Mo-2Zr-0.3Si alloy with lamellar  $\alpha + \beta$  was prepared at about 1010 °C [43] by Fournelle et al. TiAl-base alloy having lamellae structure was also produced by heat treatment (at  $1333 \pm 4$  °C) [44,45].  $\alpha_2(\text{Ti}_3\text{Al}) + \gamma(\text{TiAl})$  alloys having lamellar structure were also appeared after an annealing treatment at 1450 °C [46]. Lamellae of  $\text{Ni}_3\text{Ti}$  was prepared at high temperature as well (1100 °C) [47]. A two-phase microstructure consisting of  $\text{Pt}_3\text{Al}$  in Pt solid solution [48] and a two phase microstructure of Pt78:Al14:Ru8 alloy [49] were obtained around 1350 °C for long hours (66 hours). Materials with these micro-lamellar structures controlled by thermomechanical processes can have excellent mechanical properties [40].

The phase diagram of Cu-Zn given in Figure 5 does not show where and how the phase change occurs around room temperature as the phase diagram shows that the  $\beta'$  phase at low temperatures cannot correspond to the phase equilibrium [50]. However, this study suggests that the phase border of brass at room temperature can be similar to that of at high temperature. As  $\beta$  and  $\gamma$ -phase of brass might be solidified at  $57.50 \pm 0.50\%$  Zn content, the phase change of  $\beta$  and  $\gamma$ -phase is highlighted with red line shown in Figure 5. As brass is an important alloy used for shape memory alloy relying on the change of  $\alpha$  and  $\beta$  phases [51],  $\beta$  and  $\gamma$ -phase also can be studied even at relatively lower temperature. It has not been shown that shape memory alloy could appear for  $\beta$  phase brass (as only seen for 38.5 – 41.5 wt.% Zn content in brass [52]). This study

could be extended for the possible use of  $\beta$  brass as a shape memory alloy. However, this paper mainly focuses on the electrochemical behaviour of alloys (deposition and corrosion responses).

### 3.2.2 Corrosion Behaviour of Brass Films

Figure 6 illustrates the potentiodynamic polarization curves of pure Zn and pure Cu coating in 3wt% NaCl. Additionally, the potentiodynamic polarizations of the brass films deposited potentiostatically (applied -2 V for 300 seconds) from different electrolytes are also given in the same graph to compare with pure metal deposition in terms of corrosion resistivity. The corresponding electrochemical corrosion parameters derived from data given in Figure 6 are tabulated in Table 3.

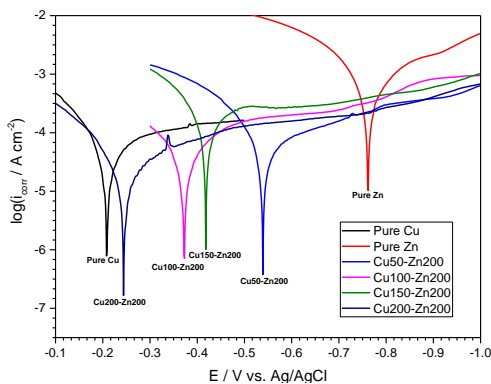


*Fig. 6: Potentiodynamic polarization curves of metals and alloys in 3wt% NaCl solution. Pure Cu, pure Zn and brasses coated from the electrolyte having different ratio of CuSO<sub>4</sub> and ZnSO<sub>4</sub> are indicated.*

The corrosion potential ( $E_{corr}$ ) of all brass deposited from different ratio of Cu in pyrophosphate medium containing constant ZnSO<sub>4</sub> is between that of pure Cu and pure Zn film deposited onto the steel. It can be deduced from the values of more positive  $E_{corr}$  and much lower  $i_{corr}$  of brasses than those of pure zinc coating that brass coating has a higher corrosion resistivity than that of the pure Zn film in 3wt% NaCl. While the  $i_{corr}$  values of the Cu50-Zn200, the Cu100-Zn200 and the Cu150-Zn200 are higher than that of pure Cu film indicating those brass are less corrosion resistive than pure copper coating, the ratio of the corrosion rate between pure Cu and the Cu200-Zn200 is more than twice meaning the Cu200-Zn200 shows less corrosive characteristic. Preparation of the brass in optimised conditions can take advantage of both metals features: more noble  $E_{corr}$  close to  $E_{corr}$  of pure Cu and much less  $i_{corr}$  than the  $i_{corr}$  values of both metals.

*Table 3: Electrochemical parameters (corrosion potential  $E_{corr}$ , corrosion current density  $i_{corr}$ ) derived from the polarization curves given in Figure 6 and ratio of Cu in the brass electrode.*

Electrolyte	Pure Zn	Cu50-Zn200	Cu100-Zn200	Cu150-Zn200	Cu200-Zn200	Pure Cu
$i_{corr}$ ( $\mu\text{A cm}^{-2}$ )	316	64.6	36.3	97.7	11.8	33.1
$-E_{corr}$ (mV vs. Ag/AgCl)	768	545	367	421	246	206
Ratio of Cu in brass	0	43	42	34	50	100

It is obvious in Table 3 that the  $i_{corr}$  of coatings decreases upon increasing the content of Cu in brass. The film obtained from the Cu150-Zn200 solution has less copper than those of the Cu50-Zn200 and the Cu100-Zn200 (indicated in section 3.2.1 and in Table 3) and the corrosion rate of the film obtained from the Cu150-Zn200 electrolyte is also higher than those of the Cu50-Zn200 and Cu100-Zn200. This shows that the corrosion rate is directly related to the content of

copper in the brass. However, the corrosion potential is independent of Cu contents as it is seen in Table 3. The difference of the potential of solid deposited from the Cu50-Zn200 and the Cu100-Zn200 is 178 mV while the Cu content in brass is almost the same.

The ratio of corrosion rate of pure Zn film to that of the film obtained from the Cu200-Zn200 is 26.8 indicating the Cu200-Zn200 film is 26.8 times more effective against corrosion than pure zinc (316/11.8 as given in Table 3) due to the effect of brass structure and the ratio content in the brass against the corrosion behaviour.

#### **4. Conclusion**

Zinc-rich brass was obtained potentiostatically from pyrophosphate electrolyte and studied potentiodynamically. The reduction of  $\text{Cu}^{2+}$  onto the carbon steel in pyrophosphate medium is directly from  $\text{Cu}(\text{P}_2\text{O}_7)_2^{6-}$  to  $\text{Cu(s)}$  at the early stage of deposition, however the mechanism later on have two steps:  $\text{Cu}(\text{P}_2\text{O}_7)_2^{6-} / \text{Cu}(\text{P}_2\text{O}_7)_2^{7-}$  and  $\text{Cu}(\text{P}_2\text{O}_7)_2^{7-} / \text{Cu}^0$ . However the striping mechanism of  $\text{Cu}^0$  for thin and thick film is the same. It is the transformation of  $\text{Cu}^0$  to  $\text{Cu}(\text{P}_2\text{O}_7)_2^{7-}$  at lower potential and  $\text{Cu}(\text{P}_2\text{O}_7)_2^{7-}/\text{Cu}(\text{P}_2\text{O}_7)_2^{6-}$  at higher potential.

The electrodeposition of  $\text{Zn}^{2+}$  in pyrophosphate medium is directly from and  $\text{Zn}(\text{P}_2\text{O}_7)_2^{6-}$  to Zn. However, the striping mechanism of Zn coating has firstly  $\text{Zn}^0/\text{Zn}(\text{P}_2\text{O}_7)_2^{7-}$  oxidation and later on the oxidation of  $\text{Zn}(\text{P}_2\text{O}_7)_2^{7-}$  to  $\text{Zn}(\text{P}_2\text{O}_7)_2^{6-}$ .

The electrodeposition of brass has both identical mechanisms of Cu and Zn deposition in the same media.  $\text{Cu}^0\text{-Zn}^0$  (alloy) is directly deposited from  $\text{Cu}(\text{P}_2\text{O}_7)_2^{6-}$  and  $\text{Zn}(\text{P}_2\text{O}_7)_2^{6-}$  onto the steel. While there is a little amount of brass on the steel substrate,  $\text{Cu}(\text{P}_2\text{O}_7)_2^{6-}$  is reduced to  $\text{Cu}(\text{P}_2\text{O}_7)_2^{7-}$  at higher potential similar to the mechanism of pure copper reduction on the steel. Brass striping from the steel has two different characteristics. The first one is for low content of zinc (<60wt%) in brass which has direct oxidation reaction of brass to  $\text{Cu}(\text{P}_2\text{O}_7)_2^{6-}$  and  $\text{Zn}(\text{P}_2\text{O}_7)_2^{6-}$ . The latter is for high content of zinc which has oxidation of Zn to  $\text{Zn}(\text{P}_2\text{O}_7)_2^{7-}$  at lower potential and  $\text{Zn}(\text{P}_2\text{O}_7)_2^{7-}/\text{Zn}(\text{P}_2\text{O}_7)_2^{6-}$  with  $\text{Cu}^0/\text{Cu}(\text{P}_2\text{O}_7)_2^{6-}$  at higher potential.

Micro-lamellar structure of brass is obtained by potentiostatic depositon of brass in pyrophosphate medium at  $20 \pm 2$  °C. This ordered structure is just observed for the brass including  $57.5 \pm 0.50$  wt% Zn at which  $\beta+\gamma$ -phase transition occurs. The ratio of Cu and Zn elements in deposited brass is not directly proportional to the contents of copper and zinc ions in the deposition electrolyte. The corrosion rate of brass decreases with increasing Cu content in solid brass. The corrosion resistivity of the Cu200-Zn200 is better than pure Cu and about 27 times higher than pure Zn.

#### **Acknowledgment**

This work was supported by a research project number of MF.09.07 from Scientific Research Projects Unit (BAPYB), Gaziantep University. The authors would like to thank Food Products R&D Center, Gaziantep University.

#### **References**

- [1] G. Kostrova, V. Obozinskaya, Sov. Electrochem. **21**, 321 (1985).
- [2] S.R. Moysan III, R.W. Sugg, US5413874 A (1995).
- [3] M. Ebrahimzadeh, M. Gholami, M. Momeni, A. Kosari, M. Moayed, A. Davoodi, Appl. Surf. Sci. **332**, 384 (2015).
- [4] H. Jie, Q. Xu, L. Wei, Y. Min, **102**, 251-258 (2016).
- [5] T. Banerjee, A. Allmand, Trans. Faraday Soc. **44**, 819 (1948).
- [6] T. Vagramyan, J. Leach, J. Moon, Electrochim. Acta **24**, 231 (1979).
- [7] A. Brenner, Electrodeposition of alloys: principles and practice, Amsterdam, Elsevier (2013).

- [8] K. Schütte, H. Meyer, C. Gemel, J. Barthel, R.A. Fischer, C. Janiak, *Nanoscale* **6**, 3116 (2014).
- [9] A.P. Abbott, K.J. McKenzie, *Phys. Chem. Chem. Phys.* **8**, 4265 (2006).
- [10] C. Domínguez-Ríos, M. Moreno, R. Torres-Sánchez, W. Antúnez, A. Aguilar-Elguézabal, J. González-Hernández, *Surf. Coat. Tech.* **202**, 4848 (2008).
- [11] A. Survila, Z. Mockus, S. Kanapeckaitė, G. Stalnionis, R. Juškėnas, V. Jasulaitienė, J. *Electrochem. Soc.* **160**, 428 (2013).
- [12] M.R.H. de Almeida, E.P. Barbano, M.G. Zacarin, M.M. de Brito, P.C. Tulio, I.A. Carlos, *Surf. and Coat. Tech.* **287**, 103 (2016).
- [13] M.A. Ibrahim, R.S. Bakdash, *Int. J. Electrochem. Sci.* **10**, 9666 (2015).
- [14] M. de Almeida, E. Barbano, M. de Carvalho, P. Tulio, I. Carlos, *Appl. Surf. Sci.* **333**, 13 (2015).
- [15] K. Johannsen, D. Page, S. Roy, *Electrochim. Acta* **45**, 3691 (2000).
- [16] V.I. Kravtsov, V.V. Kondratiev, *Electrochim. Acta* **36**, 427 (1991).
- [17] H. Konno, M. Nagayama, *Electrochim. Acta* **22**, 353 (1977).
- [18] L.F.d. Senna, S.L. Díaz, L. Sathler, *Mater. Res.* **8**, 275 (2005).
- [19] Y. Mumladze, *Sov. Electrochem.* **24**, 771 (1988).
- [20] K. Clauwaert, K. Binnemans, E. Matthijs, J. Fransaer, *Electrochim. Acta* **188**, 344 (2016).
- [21] Y. Fujiwara, H. Enomoto, *J. Electrochem. Soc.* **147**, 1840 (2000).
- [22] R. Juškėnas, V. Karpavičienė, V. Pakštas, A. Selskis, V. Kapočius, *J. Electroanal. Chem.* **602**, 237 (2007).
- [23] V.Y. Doo, R. Balluffi, *Acta metallurgica* **6**, 428 (1958).
- [24] M. Ghorbani, M. Mazaheri, K. Khangholi, Y. Kharazi, *Surf. Coat. Tech.* **148**, 71 (2001).
- [25] J. Ulaganathan, R.C. Newman, *Mater. Charact.* **92**, 127 (2014).
- [26] T. Konkova, S. Mironov, A. Korznikov, G. Korznikova, M.M. Myshlyaev, S.L. Semiatin, *Mater. Charact.* **101**, 173 (2015).
- [27] M. Hacıbrahimoglu, M. Bedir, M. Öztaş, C. Çakez, *Dig. J. Nanomater. Bio.* **10**, 1439 (2015).
- [28] M. Haghshenas, R.J. Klassen, *Mater. Sci. Eng. A* **641**, 249 (2015).
- [29] M. Öztaş, M. Bedir, *Thin Solid Films* **516**, 1703 (2008).
- [30] A.I. Toufatzis, G.A. Pantazopoulos, A.S. Paipetis, *J. Mat. Eng. Perf.* **23**, 3193 (2014).
- [31] Survila, A. in *Electrochemistry of Metal Complexes*, Wiley-VCH, Weinheim, 183 (2015)
- [32] L. Senna, S. Díaz, L. Sathler, *J. Appl. Electrochem.* **33**, 1155 (2003).
- [33] H. Strow, *Met Finish* **97**, 209 (1999).
- [34] A. Banerjee, R. Kumar, M. Dutta, S. Bysakh, A.K. Bhowmick, T. Laha, *Surf. Coat. Tech.* **262**, 200 (2015).
- [35] H. Bei, E.P. George, G.M. Pharr, *Intermetallics* **11**, 283 (2003).
- [36] S. Li, S. Zhao, M. Pan, D. Zhao, X. Chen, O. Barabash, et al., *Mater. Trans. JIM* **38**, 553 (1997).
- [37] J. Carpenter, T. Nizolek, R. McCabe, N. Mara, I. Beyerlein, T. Pollock, *Mater. Res. Lett.* **3**, 1 (2015).
- [38] C.S. Hong, N.R. Tao, X. Huang, K. Lu, *Acta Materialia* **58**, 3103 (2010).
- [39] D.P. Weston, S.P.A. Gill, M. Fay, S.J. Harris, G.N. Yap, D. Zhang, et al., *Surf. Coat. Tech.* **236**, 75 (2013).
- [40] F. Appel, M. Oehring, J.D. Paul, *Adv. Eng. Mat.* **8**, 371 (2006).
- [41] D.G. Page, *Electrodeposition of thin film shape memory alloys*, PhD Thesis, University of Newcastle (2001).
- [42] E. Çadirli, M. Gündüz, *J. Mater. Process. Technol.* **97**, 74 (2000).
- [43] A.B. Li, L.J. Huang, Q.Y. Meng, L. Geng, X.P. Cui, *Mater Des* **30**, 1625 (2009).
- [44] K.S. Chan, Y. Kim, *Acta Metallurgica Materialia* **43**, 439 (1995).
- [45] K.S. Chan, D.S. Shih, *Metallurgical and Materials Transactions A* **28**, 79 (1997).
- [46] R.M. Imayev, V.M. Imayev, M. Oehring, F. Appel, *Intermetallics* **15**, 451 (2007).
- [47] R.A. Fournelle, *Acta Metallurgica* **27**, 1135 (1979).

- [48] A. Douglas, J.H. Neethling, R. Santamarta, D. Schryvers, L.A. Cornish, *J. Alloys. Comp.* **432**, 96 (2007).
- [49] P.J. Hill, T. Biggs, P. Ellis, J. Hohls, S. Taylor, I.M. Wolff, *Mat. Sci. Eng: A* **301**, 167 (2001).
- [50] T.B. Massalski, H. Okamoto, P. Subramanian, L. Kacprzak, ASM International, **3**, 1485 (1990).
- [51] N. Haberkorn, M. Ahlers, F.C. Lovey, *Scr. Mater.* **61**, 821 (2009).
- [52] T. Massaski, H. Pops, *Trans. MetallSoc. AIME* **230**, 1662 (1964).